

## Effect of catalyst composition on carbon nanotube growth

X. Z. Liao,<sup>a)</sup> A. Serquis, Q. X. Jia, D. E. Peterson, and Y. T. Zhu  
Division of Materials Science and Technology, Los Alamos National Laboratory, Los Alamos,  
New Mexico 87545

H. F. Xu

Department of Earth and Planetary Sciences, University of New Mexico, Albuquerque, New Mexico 87131

(Received 17 January 2003; accepted 27 February 2003)

Transmission electron microscopy was used to probe the compositions of individual Co–Mo bimetal catalyst particles and the morphologies of carbon nanotubes (CNTs) catalyzed by these particles under flowing carbon monoxide at 700 °C. It was found that the composition of the catalyst particle at a CNT tip and the distribution of Co within the particle largely determine the morphology of the CNT. A particle with low Co content (<15 at. %) tends to produce a long CNT, while a particle with very high Co content (>85 at. %) tends to produce onion-like structures. These observations provide insight into the CNT growth mechanisms. © 2003 American Institute of Physics. [DOI: 10.1063/1.1569655]

Carbon nanotubes (CNTs) have attracted great interest in the scientific community because of their unique and superior chemical, physical, and mechanical properties.<sup>1–4</sup> Among the methods developed for CNT synthesis, catalytic chemical vapor deposition (CVD) tends to produce nanotubes with fewer impurities and is more amenable to large-scale processing at low cost.<sup>5,6</sup> There have been several hypotheses on how CNTs grow from a catalyst particle during the CVD.<sup>7–15</sup> One of the theories suggests that catalytic CVD involves the decomposition of carbon containing gas [hydrocarbons or carbon monoxide (CO)] on one side of a nanometer-sized catalyst particle, subsequent diffusion of carbon atoms through the volume or surface of the particle, and then precipitation of CNT on its other side.<sup>15,16</sup> This theory has been very popular, but there has been no consensus on the CNT growth mechanism. Therefore, it is of interest to have more experimental results to probe CNT growth mechanisms.

Bimetallic catalysts have been found to have catalytic synergies in producing CNTs from hydrocarbons<sup>17–20</sup> and CO.<sup>15–23</sup> The composition of a bimetallic catalyst was found to significantly affect the CNT growth. For example, when synthesizing CNTs from CO decomposition at 700 °C using Co–Mo catalysts, Kitiyanan *et al.*<sup>21</sup> and Alvarez *et al.*<sup>23</sup> found that while a catalyst with high Mo concentration is very effective in producing single-wall CNTs, Co alone tends to produce multi-walled CNTs, and Mo alone is inactive at 700 °C, although it catalyzes single-wall CNT formation at 1200 °C.<sup>15</sup> The mechanism on the synergism of bimetallic catalysts of Co and Mo has been speculated,<sup>23,24</sup> but has never been experimentally verified. Furthermore, these observations on composition effect are only qualitative, because it was based on the average initial catalyst composition. However, segregation may happen during the catalyst preparation, resulting in significant deviation of composition in an individual particle from the average composition. To quantitatively study the relationship between the catalyst composition and CNT morphology, it is essential to correlate

the compositions of individual catalyst particles with the morphologies of corresponding CNTs.

In this letter, we probe compositions and their distributions in individual Co–Mo catalyst particles and correlate them with morphologies of individual CNTs produced from decomposition of CO at 700 °C, using various transmission electron microscopy (TEM) techniques. We find three kinds of multiwalled carbon morphologies that can be credited to three composition ranges in the catalyst particles. We discuss the growth mechanisms of CNTs based on these observations.

The Co–Mo catalyst was prepared by a sol-gel process.  $\text{Co}(\text{NO}_3)_2 \cdot 6\text{H}_2\text{O}$  (cobalt nitrate) and  $(\text{NH}_4)_6\text{Mo}_7\text{O}_{24} \cdot 4\text{H}_2\text{O}$  (ammonium heptamolybdate) from Alfa Aesar were used as starting materials. Colloidal silica in methanol (Nissan Chemical Industries 3M) was mixed by magnetic stirring with a solution 1 M of cobalt nitrate and ammonium heptamolybdate with a Co:Mo:Si molar ratio of 1:2:5. In a typical experiment, after 10 min stirring a few drops of HCl were added to a 10 ml mixture and stirred for another 20 min. The gel thus formed was placed on quartz plates and dried for more than 10 h at 60 °C, forming films. The films were placed in a tubular furnace heated in Ar up to 450 °C and then calcinated in flowing Ar/H<sub>2</sub> at 700 °C for 6 h. Subsequently, the flowing gas was switched to CO and kept for 2 h. The reaction was stopped by flushing the reactor with Ar and cooled to room temperature.

TEM investigation was carried out using a JEOL 2010F operated at 200 kV and equipped with a Gatan imaging filter (GIF) system and an Oxford Instrument x-ray energy-dispersive spectroscopy (EDS) system. Quantitative EDS measurement was carried out using Co  $K\alpha$  line and Mo  $L\alpha$  line.<sup>25</sup> Elemental mapping was performed with the GIF using the three-window technique.<sup>26,27</sup> The Mo  $M_{4,5}$  edge at 227 eV in the electron energy loss spectrum was used for Mo mapping, and the centers of two pre-edge windows were set at 140 and 190 eV with a slit width of 50 eV. Co maps were obtained using the Co  $L_{2,3}$  edge at 779 eV with the centers of two pre-edge windows set at 689 and 749 eV and a larger slit width of 60 eV to increase the image intensity at higher energy loss to make it possible to focus images.

<sup>a)</sup>Electronic mail: xzliao@lanl.gov

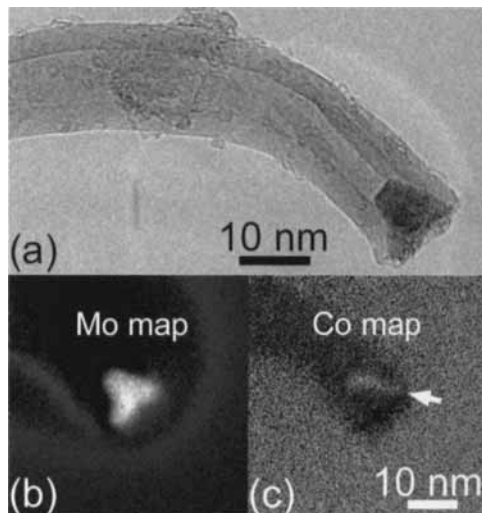


FIG. 1. (a) A high-resolution TEM showing a typical long multiwalled CNT with its catalytic particle partially exposed to environment; (b) Mo elemental map; and (c) Co elemental map showing more Co at one edge of the particle as indicated by an arrow.

Extensive high-resolution TEM investigations did not reveal any single-walled CNT in our sample, because the catalyst particle sizes are too large to form single-walled CNTs.<sup>21,23,24</sup> Instead, three kinds of multiwalled carbon morphologies were observed: (1) long CNTs, with lengths from about 0.1  $\mu\text{m}$  to a few microns, tipped with catalyst particles partially exposed to environment [see a typical example in Fig. 1(a)]; (2) short CNTs with lengths normally less than 50 nm and with catalyst particles fully encapsulated by graphene sheets [see Fig. 2(a)]; and (3) spherical, onion-shaped graphite with a catalyst particle at the center [see Fig. 3(a)]. The fact that most long CNTs observed have their catalyst particles partially exposed indicates that the direct contact of catalyst surface with carbon source is essential for

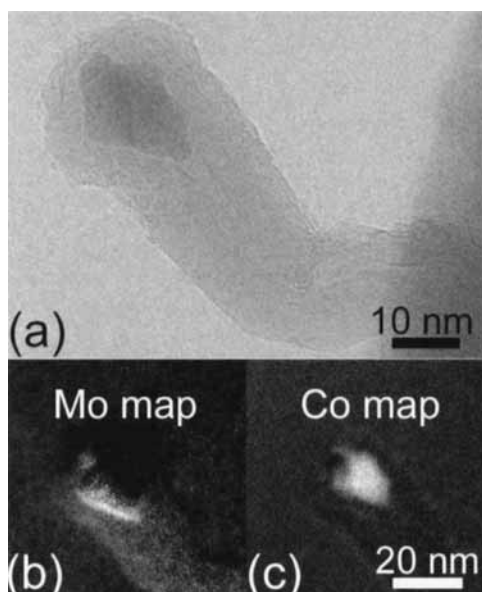


FIG. 2. (a) A high-resolution TEM showing a typical short multiwalled CNT with a catalytic particle fully encapsulated by the graphene layers; (b) Mo elemental map showing nonuniform composition distribution in the particle; and (c) Co elemental map.

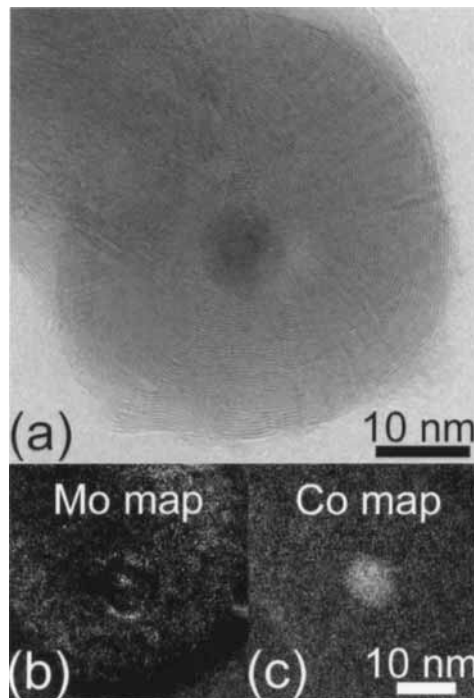


FIG. 3. (a) A high-resolution TEM showing a typical onionated multiwalled morphology with a catalytic particle located at the center of the "onion;" (b) Mo elemental map; and (c) Co elemental map.

continuous CNTs growth. This is consistent with the growth mechanism proposed by Rodriguez<sup>16</sup> and Dai *et al.*<sup>15</sup> When a catalyst particle is fully encapsulated by layers of graphene sheets, the carbon supply route is cut, and the CNT growth stops, resulting in a short CNT, as shown in Fig. 2(a). Therefore, preventing the catalyst encapsulation is a prerequisite for continuous CNT growth.

It has been reported that the sizes of metallic catalyst particles affect the CNT growth.<sup>15,28,29</sup> However, in this study, we found that the size of a catalyst particle is not a dominant factor that determines the carbon morphology, although it may have affected the formation of multiwall CNTs instead of the single-wall CNTs. For example, although the carbon morphologies in Figs. 1(a) and 3(a) are very different, their catalyst particles are very similar in size. In fact, catalyst particles with sizes much larger than that shown in Fig. 3(a) were found to catalyze long CNT formation in our sample. Kanzow and Ding<sup>7</sup> hypothesized that carbon morphology varies with the synthesis temperature. However, their theory cannot explain the morphology variations observed in our study because all three kinds of morphologies were grown under exactly the same temperature and carbon supply.

A possible factor that determines carbon morphologies is the catalyst composition. To explore this possibility, EDS and elemental mapping were carried out on up to 50 particles associated with each type of carbon morphology. EDS results indicate that the compositions of individual catalyst particles can generally be categorized into three groups, all significantly deviate from the average composition calculated from the initial Co:Mo mix ratio but generally correspond to the Co–Mo phase diagram.<sup>30</sup> There is a very clear relationship between the catalyst composition and carbon morphology.

Catalyst particles with 5–15 at. % Co tend to produce long CNTs, those with 40–45 at. % Co tend to produce short CNTs, and those with 85–98 at. % Co tend to produce onionated morphology.

The elemental mapping results in Figs. 1–3, on the other hand, suggest that the composition in a catalyst is not uniformly distributed. Severe heterogeneity in Co (or Mo) distribution in an individual particle was found to affect the carbon morphology. For example, a few particles with average Co composition of around 50 at. % produced long CNTs instead of short ones. However, elemental mapping images of these particles suggest that the Co content near the exposed particle surface is much lower than the average Co content, implying that it is the Co content on the exposed particle surface, instead of the average Co content in the whole particle, that determines the carbon morphology.

The above observations suggest that changing the Mo content in Co–Mo bimetallic catalyst can modulate the catalyst activity. Higher Mo content (lower Co content) leads to lower catalyst activity in catalyzing the decomposition of CO. When the Co content is low, the decomposition rate of CO would be low and all the released carbon atoms could diffuse to the catalyst–CNT interface for CNT growth, leaving the exposed side of the catalyst unchanged so that the CO decomposition and carbon diffusion process can be sustained for continuous CNT growth. Higher Co content in the catalyst leads to higher carbon production rate by CO decomposition than the diffusion rate. The excess carbon atoms will accumulate on the initially exposed side of the catalyst particle and form graphene layers. The CNT stops growth once graphene layers completely cover the initially exposed side of the catalyst particle, which cuts off the carbon supply route, resulting in a short CNT. When a catalyst particle contains very high Co content, high rate CO decomposition simultaneously occurs on the whole surface of the particle, quickly forming onionated structure without nucleating CNT. It should be noted that when the Co atom distribution is heterogeneous within a catalyst particle, it is the Co content near the exposed particle surface that determines the CO decomposition rate, and consequently the CNT length.

Adjusting the CO supply (CO partial pressure) has the same effect as varying catalyst composition in providing carbon for CNT growth. For example, Alvarez *et al.*<sup>23</sup> reported that, by using CO diluted with 50% He, Co catalyzed multi-walled CNT formation while Mo catalyst was inactive at 700 °C. Valentini *et al.*<sup>31</sup> used CH<sub>4</sub>/N<sub>2</sub> mixture and Ni catalyst to produce CNTs, and found well-aligned CNTs when the CH<sub>4</sub>:N<sub>2</sub> ratio was low and no CNTs for pure CH<sub>4</sub> gas. These observations are consistent with the CNT growth mechanism observed in our study. The decomposition rate of CO or CH<sub>4</sub> increases with its partial pressure. Diluting CO (or CH<sub>4</sub>) leads to lower decomposition rate, and therefore lower production rate of carbon atoms. This prevents the accumulation of excess carbon atoms on the catalyst particles. There are also several other studies that are consistent with the earlier discussions.<sup>24,29,32</sup>

In summary, we have correlated the Co–Mo composition and its distribution in each individual catalyst particle with the morphology of the corresponding carbon product. The results show that the Co–Mo catalyst composition deter-

mines the morphology of carbon product. To synthesize long CNTs, it is critical to balance the rate of CO decomposition and the rate of carbon atom diffusion so as to keep the carbon supply route open. The rate of carbon diffusion will be affected mostly by the synthesis temperature, while the CO decomposition rate will be affected by both the synthesis temperature and the CO partial pressure. Therefore, for a selected Co–Mo bimetallic catalyst, both synthesis temperature and CO partial pressure need to be optimized to produce long CNTs.

This work was performed under the auspices of the US Department of Energy. The JEOL 2010F in the University of New Mexico is funded by the NSF (CTS98-71292). H.F.X. thanks support from NSF (EAR02-10820).

- <sup>1</sup>A. C. Dillon, K. M. Jones, T. A. Bekkedahl, C. H. Kiang, D. S. Bethune, and M. J. Heben, *Nature (London)* **386**, 377 (1997).
- <sup>2</sup>T. W. Odom, J. L. Huang, P. Kim, and C. M. Lieber, *Nature (London)* **391**, 62 (1998).
- <sup>3</sup>M. M. J. Treacy, T. W. Ebbesen, and J. M. Gibson, *Nature (London)* **381**, 678 (1996).
- <sup>4</sup>J. P. Lu, *Phys. Rev. Lett.* **74**, 1123 (1995).
- <sup>5</sup>R. K. Rana, Y. Kolytyn, and A. Gedanken, *Chem. Phys. Lett.* **344**, 256 (2001).
- <sup>6</sup>E. T. Thostenson, Z. Ren, and T. W. Chou, *Compos. Sci. Technol.* **61**, 1899 (2001).
- <sup>7</sup>H. Kanzow and A. Ding, *Phys. Rev. B* **60**, 11180 (1999).
- <sup>8</sup>C. Ducati, I. Alexandrou, M. Chhowalla, G. A. J. Amaratunga, and J. Robertson, *J. Appl. Phys.* **92**, 3299 (2002).
- <sup>9</sup>X. Zhang, A. Cao, B. Wei, Y. Li, J. Wei, C. Xu, and D. Wu, *Chem. Phys. Lett.* **362**, 285 (2002).
- <sup>10</sup>Y. J. Yoon and H. K. Baik, *Diamond Relat. Mater.* **10**, 1214 (2002).
- <sup>11</sup>A. Gorbunov, O. Jost, W. Pompe, and A. Graff, *Carbon* **40**, 113 (2002).
- <sup>12</sup>J. Gavillet, A. Loiseau, F. Ducastelle, S. Thair, P. Bernier, O. Stéphan, J. Thibault, and J.-C. Charlier, *Carbon* **40**, 1649 (2002).
- <sup>13</sup>A. Louchev, Y. Sato, and H. Kanda, *Appl. Phys. Lett.* **80**, 2752 (2002).
- <sup>14</sup>N. S. Kim, Y. T. Lee, J. Park, H. Ryu, H. J. Lee, S. Y. Choi, and J. Choo, *J. Phys. Chem. B* **106**, 9286 (2002).
- <sup>15</sup>H. Dai, A. G. Rinzler, P. Nikolaev, A. Thess, D. T. Colbert, and R. E. Smalley, *Chem. Phys. Lett.* **260**, 471 (1996).
- <sup>16</sup>N. M. Rodriguez, *J. Mater. Res.* **8**, 3233 (1993).
- <sup>17</sup>C. H. Kiang, W. A. Goddard III, R. Beyers, J. S. Salem, and D. S. Bethune, *J. Phys. Chem. Solids* **57**, 35 (1996).
- <sup>18</sup>E. Flahaut, A. Govindaraj, A. Peigney, C. H. Laurent, A. Rousset, and C. N. R. Rao, *Chem. Phys. Lett.* **300**, 236 (1999).
- <sup>19</sup>A. M. Cassell, J. A. Raymakers, J. Kong, and H. Dai, *J. Phys. Chem. B* **103**, 6484 (1999).
- <sup>20</sup>M. Su, B. Zheng, and J. Liu, *Chem. Phys. Lett.* **322**, 321 (2000).
- <sup>21</sup>B. Kitiyanan, W. E. Alvarez, J. H. Harwell, and D. E. Resasco, *Chem. Phys. Lett.* **317**, 497 (2000).
- <sup>22</sup>A. Lan, Z. Iqbal, A. Aitouchen, M. Libera, and H. Grebel, *Appl. Phys. Lett.* **81**, 433 (2002).
- <sup>23</sup>W. E. Alvarez, B. Kitiyanan, A. Borgna, and D. E. Resasco, *Carbon* **39**, 547 (2001).
- <sup>24</sup>J. E. Herrera, L. Balzano, A. Borgna, W. E. Alvarez, and D. E. Resasco, *J. Catal.* **204**, 129 (2001).
- <sup>25</sup>H. F. Xu and Y. F. Wang, *J. Nucl. Mater.* **279**, 100 (2000).
- <sup>26</sup>L. Reimer, *Energy-Filtering Transmission Electron Microscopy* (Springer, Berlin, 1995), p. 347.
- <sup>27</sup>X. Z. Liao, J. Zou, D. J. H. Cockayne, J. Wan, Z. M. Jiang, G. Jin, and K. L. Wang, *Phys. Rev. B* **65**, 3306 (2002).
- <sup>28</sup>Y. Y. Wei, G. Eres, V. I. Merkulov, and D. H. Lowndes, *Appl. Phys. Lett.* **78**, 1394 (2001).
- <sup>29</sup>E. F. Kukovitsky, S. G. L'vov, N. A. Sainov, V. A. Shustov, and L. A. Chernozatonskii, *Chem. Phys. Lett.* **355**, 497 (2002).
- <sup>30</sup>E. A. Brandes and G. B. Brook, *Smithells Metals Reference Book*, 7th ed. (Butterworth-Heinemann, Oxford, 1992), Chap. 11, p. 197.
- <sup>31</sup>L. Valentini, J. M. Kenny, L. Lozzi, and S. Santucci, *J. Appl. Phys.* **92**, 6188 (2002).
- <sup>32</sup>L. Alvarez, T. Guillard, J. L. Sauvajol, G. Flamant, and D. Laplaze, *Chem. Phys. Lett.* **342**, 7 (2001).